Natural Vanadium–Titanium Magnetite Activated Peroxydisulfate and Peroxymonosulfate for Acid Orange II Degradation: Different Activation Mechanisms and Influencing Factors

Zheng Zhang [1], Libin Zhao [2,3], Jingyuan Tian [1], Shaojie Ren [2,3,*] and Wei Zhang [2,3]

[1] Henan Academy of Geology, No. 16 Jinshui East Road, Zhengzhou 450016, China
[2] School of Ecology and Environment, Zhengzhou University, 100 Kexue Avenue, Zhengzhou 450001, China
[3] Henan International Joint Laboratory of Water Cycle Simulation and Environmental Protection, Zhengzhou 450001, China
* Correspondence: rsj@zzu.edu.cn

Abstract: Persulfate-based advanced oxidation processes have emerged as a promising approach for the degradation of organic pollutants in aqueous environments due to their ability to generate sulfate radicals ($SO_4^{-\cdot}$) within catalytic systems. In this study, peroxydisulfate (PDS) and peroxymonosulfate (PMS) were investigated with the natural vanadium–titanium magnetite (VTM) as the activator for the degradation of acid orange II. The degradation efficiency increased with higher dosages of VTM or persulfate (both PDS and PMS) at lower concentrations (below 10 mM). However, excessive PMS (higher than 10 mM) in the PMS/VTM system led to the self-consumption of free radicals, significantly inhibiting the degradation of acid orange II. The VTM-activated PDS or PMS maintained an effective degradation of acid orange II in a wide pH range (3~11), suggesting remarkable pH stability. The $SO_4^{-\cdot}$ was the main active species in the PDS/VTM system, while hydroxyl radical (·OH) also contributed significantly to the PMS/VTM system. In addition, PMS exhibited better thermal stability during VTM activation. Coexisting ions in an aqueous environment such as bicarbonate (HCO_3^-), carbonate (CO_3^{2-}), and hydrogen phosphate (HPO_4^{2-}) had obvious effects on persulfate activation. Our study systematically investigated the different activation processes and influencing factors associated with PDS and PMS when the natural VTM was used as a catalyst, thereby providing new insights into the persulfate-mediated degradation of organic pollutants in aqueous environments.

Keywords: vanadium–titanium magnetite; persulfate; sulfate radical; advanced oxidation process; coexisting ions

1. Introduction

The advancement of industrialization has led to a significant increase in organic contaminants within aquatic ecosystems, posing a considerable risk to human health [1,2]. Conventional biological treatment methods, such as activated sludge systems and constructed wetlands, have proven inadequate for the effective removal of these contaminants [3]. Advanced oxidation processes (AOPs) employ highly reactive radicals to degrade the organic pollutants [4–6]. Commonly, AOPs, including the Fenton reaction [7], photocatalysis [8,9], and electrocatalysis [10,11], primarily rely on hydroxyl radicals (·OH) for their efficacy. Owing to the high reactivity and minimal self-scavenging properties [12], alternative AOPs utilizing sulfate radical ($SO_4^{-\cdot}$) have drawn significant attention in pollutants mitigation [13,14].

In sulfate radical-based AOPs, sulfate radicals exhibit a significantly higher redox potential (E0 = 2.5–3.1 V), which is more desirable than hydroxyl radicals (E0 = 1.8–2.7 V) toward electron-rich recalcitrant contaminants [15,16]. Persulfate, including peroxydisulfate

(PDS) and peroxymonosulfate (PMS), could serve as a precursor for the generation of sulfate radicals [17,18]. The peroxide bond could be cleaved by metal ions [19], thermo [20], and ultraviolet radiation [21]. Previous research has shown that heating is an effective method for activating PDS or PMS [22]. Transition metal ions and metal oxides have been shown to effectively activate PDS and PMS to degrade organic pollutants [23,24]. Compared with transition metals, the Fe element is noted for its environmental friendliness, non-toxicity, and cost-effectiveness, making it a common choice for persulfate activation [21,25]. Natural vanadium–titanium magnetite, which is doped with various metal elements such as iron, manganese, and titanium [26–28], not only possesses conventional adsorption properties but also functions as an activator of persulfate to generate sulfate radical [29,30]. Acid orange II, which contains azo functional groups and a naphthalene structure, is the largest class of synthetic dyes used in the textile industry. It has caused serious ecological and environmental problems due to the toxicity, non-biodegradability, and potential carcino-genicity [31]. Previous research indicated that the acid orange II could be degraded by AOPs effectively [32,33]. Thus, this is an effective strategy for the degradation of acid orange II through VTM-activated persulfate.

Gauging the true potential of persulfate oxidation technology for organic pollutant treatment in aqueous environments requires a careful evaluation of complex factors such as activation mechanisms and water matrix effects of persulfate. In persulfate activation systems, the unique reactivity of PMS/PDS and the involvement of dominant radicals are significantly different under various aqueous environments [34]. Previous research has indicated that when copper oxide is used as an activator, the dominant reactive species in the PDS system depends on pH conditions; specifically, sulfate radicals predominate in acidic conditions, while hydroxyl radicals are favored in alkaline conditions [35]. Furthermore, elevated temperatures may promote the occurrence of side reactions such as sulfate radical or hydroxyl radical recombination, reducing the removal efficiency of organic pollutants [36]. Therefore, a systematic investigation into the activation mechanisms of various persulfate systems is necessary to explore the potential effects of complex aqueous condition factors.

In this study, natural VTM was employed to activate different persulfates (PDS and PMS). A comprehensive analysis of the microstructure and elemental composition of VTM was conducted to elucidate the potential activation mechanisms for persulfate. The distinct activation mechanisms of PMS and PDS by VTM were explored through the comparative analysis of the degradation characteristics of organic dye acid orange II. The primary degradation mechanisms of acid orange II were assessed under multiple aqueous environmental conditions. Meanwhile, the influence of coexisting ions and free radicals was explored to analyze the potential differences between PDS and PMS activation. Our study provided a valuable exploration of the persulfate activation and highlighted the potential application of persulfate-based advanced oxidation to degrade organic pollutants in complex aqueous environments.

2. Materials and Methods

2.1. Materials

Acid orange II was purchased from Yousuo Chemical Reagent Co., Ltd., Linyi, China. Sodium persulfate ($Na_2S_2O_8$) was obtained from Kemiou Chemical Reagent Co., Ltd., Tianjin, China. Potassium peroxymonosulfate ($KHSO_5 \cdot 0.5KHSO_4 \cdot 0.5K_2SO_4$) was supplied by Aladdin Biochemical Technology Co., Ltd., Shanghai, China.

2.2. Characterizations of VTM

The samples of natural VTM were collected from the Pan-Xi region, in Sichuan Province, China. The samples were ground and passed through a 100-mesh screen. The morphology and surface structure of VTM were observed by field emission scanning electron microscopy (SEM, Zeiss, Germany). The distribution of main elements (Fe and Ti) was measured by an energy dispersive X-ray spectrometer (EDS, Zeiss, Germany) with the atomic-resolution chemical mapping method. The crystalline structure and chemical

components of VTM were investigated by X-ray diffraction technique (XRD, Empyrean, PANalytical, NLD, Worcestershire, UK). The chemical compositions of VTM were also analyzed by X-ray photoelectron spectroscopy (XPS, Escalab 250Xi, Thermo Scientific, Waltham, MA, USA). The porous properties, surface area, and pore size distribution of VTM were analyzed by Brunauer–Emmett–Teller (BET, ASAP3020, Micromeritics, Norcross, GA, USA).

2.3. Acid Orange II Decolorization Analysis

The acid orange II (0.1 mM and 200 mL) decolorization test was conducted at a temperature of $23 \pm 2\ °C$ with 300 r/min shaking. The single variable method was used to explore the effects of different oxidants and environmental factors on the degradation of acid orange II. First, the concentration of oxidants (PDS or PMS) was 10 mM with the various VTM concentrations (0–1.6 g). Acid orange II was detected based on the previous study; after filtration with a 0.45 μm membrane, the concentration of acid orange II was tested at 484 nm by using a spectrophotometer (UV759CRT, Shanghai Youke Instrument CO., LTD, Shanghai, China) [37]. The degradation efficiency of acid orange II can be calculated by Equation (1).

$$Decolorization\ efficiency\ (\%) = \frac{C_0 - C}{C_0} \times 100\% \tag{1}$$

where C_0 is the initial concentration of the acidic orange II solution, and C is the concentration of the acidic orange II solution in the collected sample.

Subsequently, the decolorization of acid orange II was determined at different oxidant concentrations. The dosages of PDS or PMS were 0, 1, 2, 5, 10, 20, 30, and 40 mM, respectively. In order to explore the effect of different pH on the degradation of acid orange II, experimental conditions (VTM 0.4 g, PDS 10 mM, and PMS 10 mM) were used. NaOH and H_2SO_4 solutions were used to adjust the pH of the reaction system.

2.4. Exploration of Degradation Mechanism

2.4.1. Free Radical Quenching Experiment

Anhydrous ethanol (EtOH) and tert-butyl alcohol (TBA) were used as free radical quenchers to explore the activation mechanism of PDS/PMS by VTM at different conditions. Different concentrations of EtOH (0 to 3.0 mmol/L) and TBA (0 to 2.0 mmol/L) were added to the oxidative degradation system. Then, the degradation rate of acid orange II was measured.

2.4.2. Coexisting Ion Effects on the Activation of PDS/PMS by VTM

For investigating the effect of coexisting ions in natural water on the degradation of acid orange II by VTM-activated PDS/PMS, several ions commonly found in natural water, including Cl^-, NH_4^+, HCO_3^-, CO_3^{2-}, Mg^{2+}, Al^{3+}, and HPO_4^{2-}, were selected to explore their interference with the catalytic degradation system. Acid orange II degradation experiments with different concentration ions (0, 1, 10, and 100 mM) were conducted under the specified reaction conditions of VTM (0.4 g), PDS or PMS (2 mM). The concentration of acid orange II in the collected samples was detected to analyze the change in activation efficiency of PDS or PMS by VTM.

3. Results and Discussion

3.1. Characterization of VTM

3.1.1. Microstructure and Chemical Analysis

The morphology and chemical composition of the VTM were analyzed by the SEM and EDS analyses (Figure 1). The VTM exhibited a smooth surface, potentially causing poor adsorption capacity. XRD diffraction measurements were conducted to examine the nature of the crystallinity of the VTM (Figure 2a). The primary component of the VTM was identified as magnetite according to the standard JCPDS 019-0629 ($2\theta = 24.138°$, $33.153°$,

35.612°, 39.277°, 43.519°, 49.480°, 57.429°, and 62.451°), which can be attributed to the natural magnetite with spinel structure. In addition, due to the low concentrations of vanadium (V) and titanium (Ti), these elements were not detectable in the XRD analysis.
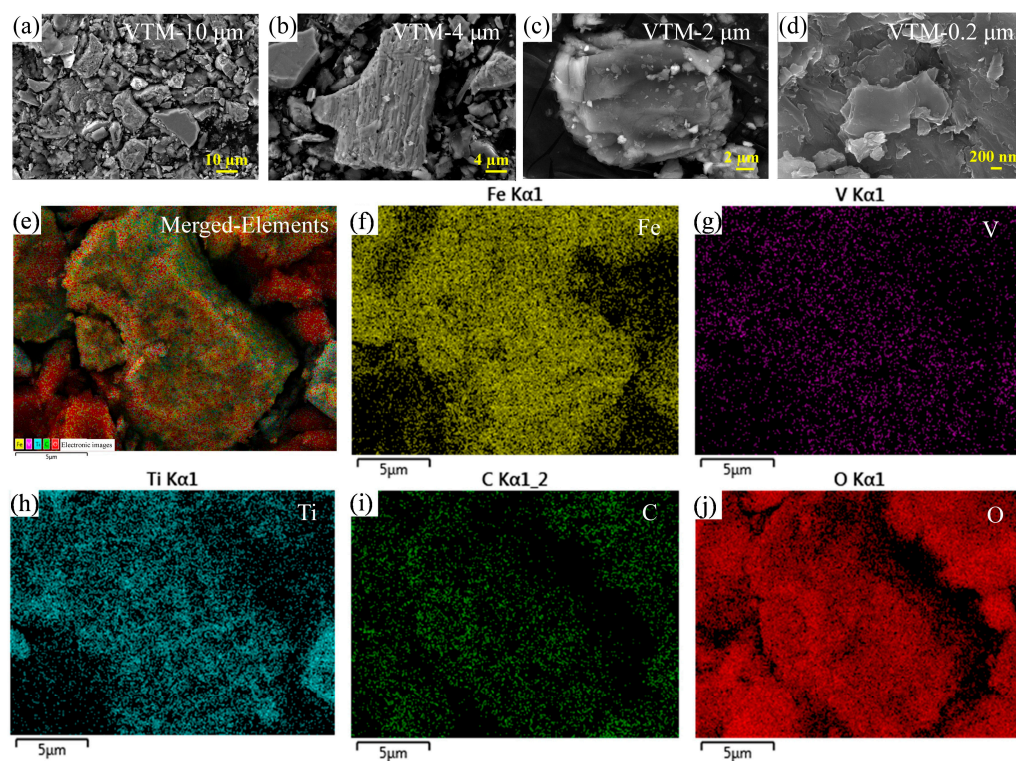

Figure 1. SEM and EDS mapping images of the VTM. (**a**–**d**) Surface morphology of VTM at different resolutions. EDS results of different elements on the VTM surface: (**e**) merged image, (**f**) Fe, (**g**) V, (**h**) Ti, (**i**) C, and (**j**) O elements.
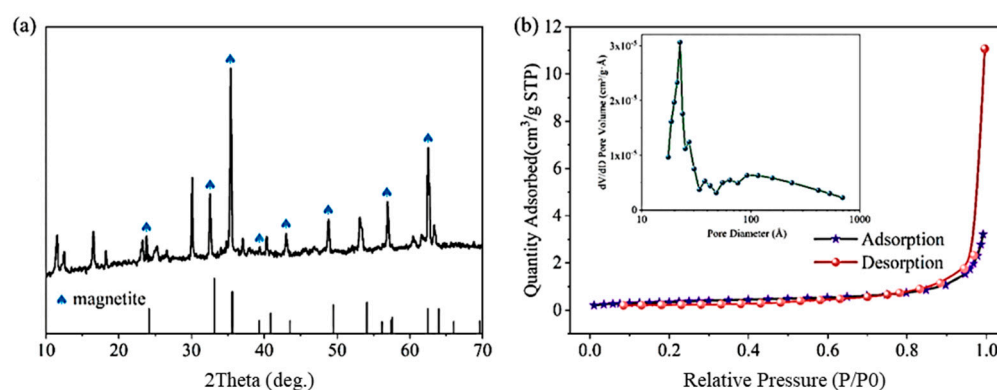

Figure 2. (**a**) XRD patterns **of** the VTM. (**b**) Nitrogen adsorption−desorption isotherms; inset image was the pore size distribution of the VTM.

The specific surface area and pore size of the VTM were measured through nitrogen adsorption–desorption isotherms. As illustrated in Figure 2b, the isotherm did not display a pronounced upward convexity at low relative pressures. The presence of a hysteresis loop at elevated relative pressures suggested that the catalyst possessed irregular mesopores. The analysis revealed a narrow pore size of 30.6 angstroms and a broader aperture range of 17.4 to 695.4 angstroms, which can be attributed to the irregular size and shape of the pores within the aggregated VTM particles [38,39]. In addition, the porosity of VTM was 4.33 g/cm^3, with a bulk density of 1.29 g/cm^3, resulting in a porosity of 70.11%.

3.1.2. XPS Analysis of VTM

The elemental valence bond composition of VTM was investigated by the XPS analysis (Figure 3). XPS is a non-destructive surface analysis technique with a detection depth of around 5–10 nm, revealing the relative content of elements in the samples. The binding energy was calibrated with a C1s peak of 284.8 eV [40], followed by peak fitting for analyzing the functional groups on the natural VTM surface. The peaks at 709.02 eV and 722.12 eV can be attributed to the presence of Fe^{2+}. The peaks at 710.21 eV and 723.31 eV were observed at VTM indicating the presence of Fe^{3+}. In addition, the typical Fe 2p3/2 and Fe 2p1/2 peaks located at 707.71 and 720.10 eV may correspond to Fe-S [41,42], since the S element was detected in the original natural-VTM before the reaction (Table S1). The VTM was identified as the ferrite compound, with a decrease in the Fe^{2+} content and an increase in the Fe^{3+} content observed following the degradation process of acid orange II. The XPS peak spectra of VTM before and after the reaction were slightly shifted compared to the standard peaks, which may be related to the complexity of the natural VTM. From the full-range scan of XPS, the decrease in the elements was observed after the reaction, such as Mg (from 11.48 atom% to 5.95 atom%) and Al (from 9.64 atom% to 7.73 atom%). Meanwhile, the ratios of the main metal elements of VTM were significant, such as Fe (from 1.00 atom% to 6.99 atom%) and Ti (from 0.13 atom% to 2.36 atom%). The changes in the composition of VTM due to the release of surface elements are also clearly reflected in the XPS results. We further made inferences about the O1s on the VTM surface based on the main elemental composition. The results indicate that the peaks at 529.58 eV could be attributed to the Ti-O, Fe-O bond [43] or lattice oxygen peak [44], the peak at nearly 531 $\pm$0.1 eV could be regarded as an Al-O bond, and the peak at 531.8 eV could be assumed as a Si-O bond due to a slight peak shift. The peaks at 531.58 eV corresponded to the C-O bond within the transition metal layer. In the C1s spectrum, the peaks at 285.4 and 288.84 eV were attributed to C–O and C=O, respectively [45]. The relative amount of C=O bond was decreased owing to the oxidation effect of reactive generated by VTM-activated PDS/PMS after the reaction. The significant changes in Fe and O elements also indicated that both of them are involved in the removal of acid orange II by the VTM-activated persulfate reaction.
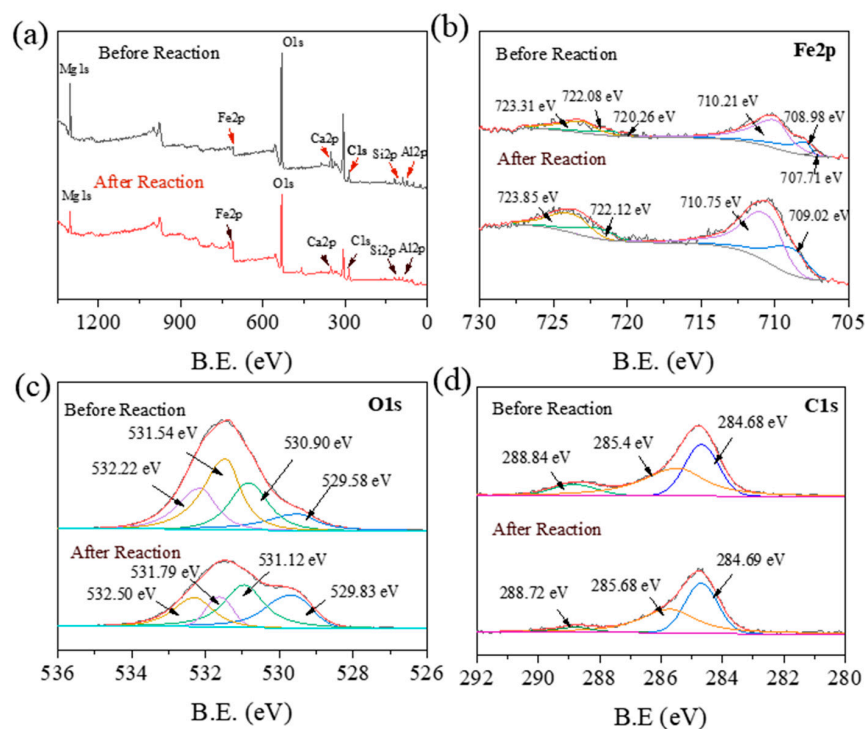

Figure 3. XPS spectra of the VTM before and after acid orange II degradation tests: (**a**) full-range scan, (**b**) Fe 2p spectra, (**c**) O 1s spectra, and (**d**) C 1s spectra.

3.2. Degradation of Acid Orange II Under Different Conditions

3.2.1. Effects of VTM Dosage on Acid Orange II Degradation

The concentration of VTM plays an important role in the activation of PDS and PMS. As shown in Figure 4a,b, there were no significant alterations in the concentration of acid orange II when PDS or PMS was utilized independently, without the presence of VTM. The degradation efficiency of acid orange II in the PDS/VTM system reached 45.5% after 60 min with 0.1 g/L VTM added. However, when the VTM dosage was 0.2 g/L, the degradation efficiency of acid orange II increased to 75.4%. Further increasing the VTM concentration to 0.5 g/L resulted in nearly complete degradation of acid orange II after 60 min. Similarly, in the PMS/VTM system, the degradation efficiency of acid orange II also increased with the VTM concentration. However, its degradation efficiency was much lower than that observed in the PDS/VTM system. When the VTM concentration was 0.1 g/L, the degradation efficiency of acid orange II was only 11%. When the VTM dosage was 0.5 g/L, there was only a 45% degradation of acid orange II. Fe(II) is the primary agent responsible for activating PDS and PMS to generate $SO_4^{-\cdot}$. As the source of Fe(II), the amount of activator VTM can significantly affect the degradation efficiency. Elevated VTM concentrations can enhance the activation of PDS and PMS, thereby generating a greater number of reactive species (Reactions (2) and (3)) [46]. However, in the PDS/VTM system, the decreased degradation efficiency of acid orange II was observed when the VTM dosage increased from 2.0 g/L to 8.0 g/L. The addition of excessive VTM led to the unfavorable recombination of active species $SO_4^{-\cdot}$, as reaction (4) inhibited the degradation of acid orange II. In addition, the $SO_4^{-\cdot}$ may react with extra Fe(II) (Reaction (5)) [47], causing the additional consumption of active substances.
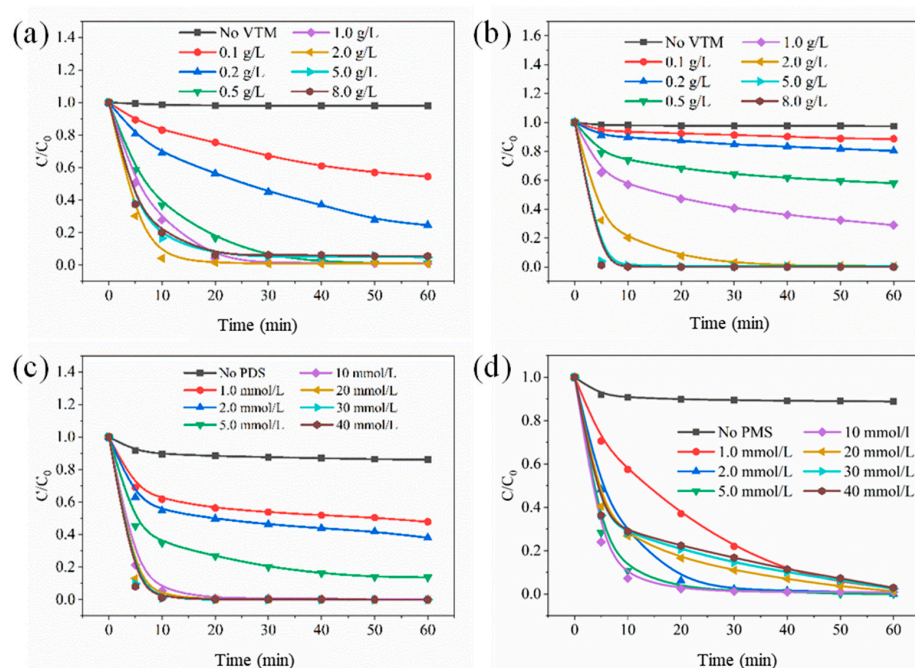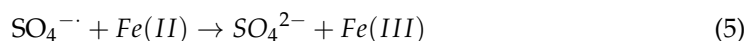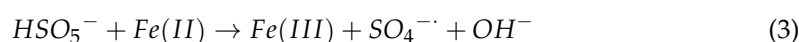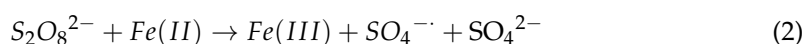
$$S_2O_8{}^{2-} + Fe(II) \rightarrow Fe(III) + SO_4^{-\cdot} + SO_4{}^{2-} \tag{2}$$

$$HSO_5{}^- + Fe(II) \rightarrow Fe(III) + SO_4^{-\cdot} + OH^- \tag{3}$$

$$SO_4^{-\cdot} + SO_4^{-\cdot} \rightarrow 2SO_4{}^{2-} \tag{4}$$

$$SO_4^{-\cdot} + Fe(II) \rightarrow SO_4{}^{2-} + Fe(III) \tag{5}$$

Figure 4. Effect of VTM dosage on the acid orange II degradation in (**a**) VTM/PDS system and (**b**) VTM/PMS system. Effect of (**c**) PDS and (**d**) PMS concentrations on the acid orange II degradation efficiency.

However, owing to the lower activation efficiency of VTM on PMS, no corresponding decrease in the degradation rate of acid orange II was observed in the PMS/VTM system with excessive VTM usage. Considering both the efficiency and cost implications of the activator, a VTM dosage of 2.0 g/L was selected for subsequent experiments.
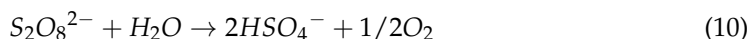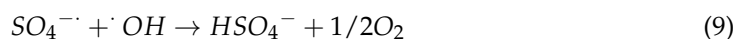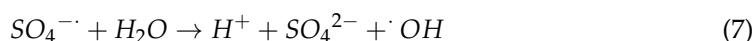
3.2.2. Effect of PDS or PMS Dosage

As shown in Figure 4c,d, minimal degradation of acid orange II occurred when only VTM was introduced into the reaction system. This rapid removal of acid orange II within ten minutes may be due to the adsorption effect of VTM. The degradation efficiency of acid orange II exhibited an increase in response to higher concentrations of PDS or PMS. When the concentration of PDS increased from 0 to 1.0 mM, the degradation efficiency of acid orange II increased significantly from 13.8% to 52.1%. Further increases in PDS concentration to 10 mM or more resulted in the complete degradation of acid orange II within 30 min (Figure 4c). Compared to PDS, when the concentration of PMS was 1.0 mM, the degraded efficiency reached 97.0% after 60 min, indicating that VTM provided a higher activation efficiency for PMS (Figure 4d). However, when the PMS concentration exceeded 10 mM, a decrease in the degradation efficiency of acid orange II was observed, attributed to the adverse consumption of active species (Reaction (6)) [48]. Based on these findings, subsequent experiments exploring degradation mechanisms and the influence of environmental factors utilized 2.0 mM concentrations of either PDS or PMS.

$$SO_4^{\cdot -} + HSO_5^- \rightarrow SO_5^{\cdot -} + SO_4^{2-} + H^+ \tag{6}$$
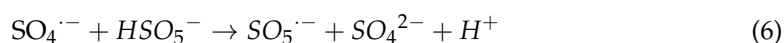
3.2.3. Effect of pH, Temperature, and Coexisting Ions on the Reaction System

The activation of PDS/PMS by VTM was influenced by the pH of the reaction system. As illustrated in Figure 5, within the VTM/PDS reaction system, the degradation profiles of acid orange II were nearly identical across a range of initial pH values from 3 to 11, suggesting that the pH had minimal impact on the activation efficiency of VTM for PDS. The $SO_4^{-\cdot}$ generated in the reaction process can react with the H_2O or OH^-, causing the formation of H^+ and decreasing the pH of the reaction system (Reactions (7) to (10)). Finally, despite variations in initial pH, the pH of the reaction system converged to a similar value within the range of pH 3 to 11 (inset image, Figure 5a). It is worth noting that in the VTM/PMS system, when the initial pH of the solution was 1.0, the degradation efficiency of the acid orange II was lower (~82%) than that at other pH levels (Figure 5b). This indicates that the pH of the reaction system has a negligible effect on VTM-activated PDS/PMS, suggesting that the activation process is applicable across a broad pH range (11).

$$SO_4^{-\cdot} + H_2O \rightarrow H^+ + SO_4^{2-} + {}^{\cdot}OH \tag{7}$$

$$SO_4^{-\cdot} + OH^- \rightarrow SO_4^{2-} + {}^{\cdot}OH \tag{8}$$

$$SO_4^{-\cdot} + {}^{\cdot}OH \rightarrow HSO_4^- + 1/2O_2 \tag{9}$$

$$S_2O_8^{2-} + H_2O \rightarrow 2HSO_4^- + 1/2O_2 \tag{10}$$

$$HSO_4^- \rightarrow SO_4^{2-} + H^+ \tag{11}$$

Temperature is an important parameter influencing PDS/PMS activation. As shown in Figure 5c,d, different temperatures (25 to 55 °C) had little effect on the degradation efficiency of acid orange II in the VTM/PDS reaction system which may be related to the faster active reaction in this system. In addition, when there was no PDS/PMS present, acid orange II did not degrade at 55 °C for 60 min, suggesting that the acid orange II was its relative stability and lack of spontaneous decomposition under elevated temperature conditions. In the PDS system, acid orange II exhibited an obvious degradation process (83.7%) even without VTM, indicating that this temperature was sufficient to activate PDS and generate active radicals. Conversely, in the PMS reaction system acid orange II was not substantially degraded (15%) at the same temperature (55 °C) without VTM. PDS and

PMS had different molecular structures. The dissociation energy of the O-O in PMS is 377 kJ/mol, while 92 kJ/mol in PDS [49,50]. Thus, PMS is more difficult to be thermally activated compared to PDS.
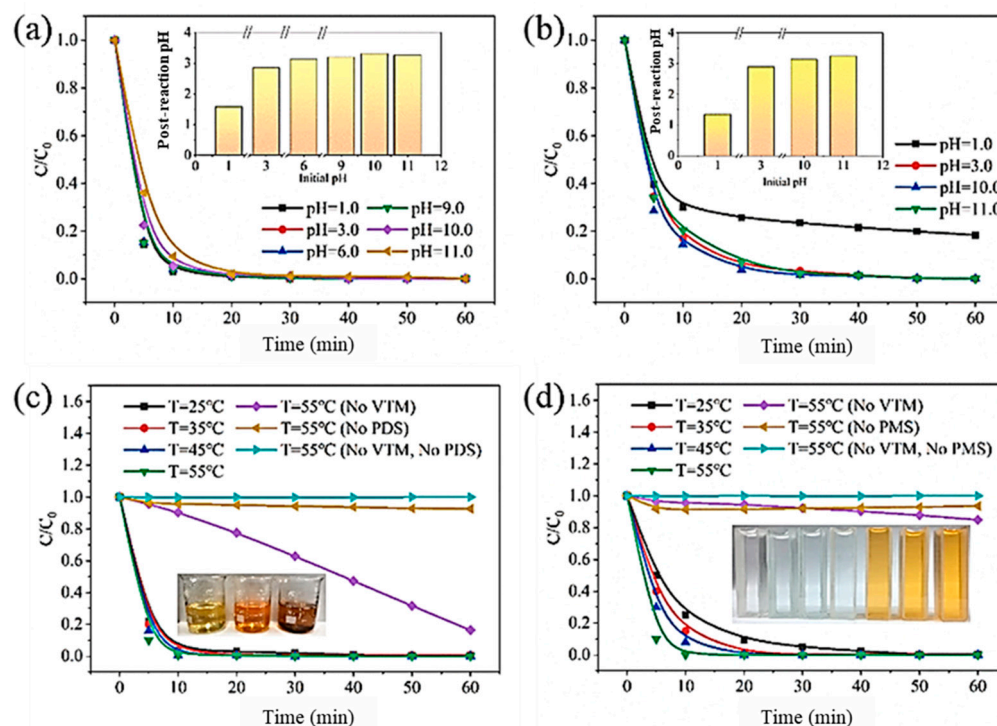

Figure 5. Effect of different initial pH on the degradation efficiency of acid orange II in the (**a**) VTM/PDS system and (**b**) VTM/PMS system. The inset image is the final pH after a 60 min reaction. Effect of different temperatures on the degradation efficiency of acid orange II in the (**c**) VTM/PDS system and (**d**) VTM/PMS system. The inset image is the color change in the acid orange II after a 60 min reaction.

Furthermore, the presence of coexisting ions in the aqueous solution may affect the activation efficiency of PDS/PMS with VTM [51]. A comprehensive investigation was conducted on various ions, including Cl^-, NH_4^+, HCO_3^-, CO_3^{2-}, Mg^{2+}, Al^{3+}, and HPO_4^{2-}. It was observed that as the concentration of these ions increased, their inhibitory effect on the degradation of acid orange II also intensified. In the PDS/VTM system, it was found that the HCO_3^-, CO_3^{2-}, and HPO_4^{2-} exhibited a significant influence on the acid orange II degradation (Figure S1). These ions could consume the active free radicals generated in the system, thereby reducing the occurrence of oxidation. Moreover, when the CO_3^{2-} and HPO_4^{2-} concentrations were higher than 10 mM, the degradation rate of acid orange presented a slight increase, which can be attributed to the change in pH of the reaction system during a large amount of ions addition [52]. For the PMS/VTM system, it was found that HCO_3^- and HPO_4^{2-} presented a significant influence on the acid orange II degradation (Figure S2). Consistent with the findings in the PDS/VTM system, the degradation efficiency of acid orange II decreased with rising ionic concentrations (NH_4^+, Mg^{2+}, and Al^{3+}). However, the high concentration (100 mM) of HCO_3^{2-} and HPO_4^{2-} increased the reaction rate compared to a lower ionic strength of 10 mM.

3.3. Analysis of Degradation Mechanisms by the PDS/PMS with VTM

The primary mechanism underlying the degradation of acid orange II involves the activation of PDS/PMS by VTM, which leads to the release of oxidative free radicals. Here, EtOH and TBA were applied to explore the influence of active free radicals in the reaction system (Figure 6). The reaction rates of EtOH and TBA with $SO_4^{-·}$ and

$\cdot$OH were markedly different. Previous research indicated that the rate constant of the reaction between EtOH and $\cdot$OH is 1.2~2.8 $\times$ 10^9 M^{-1}s^{-1}, and the rate constant of reaction with SO$_4^-$ is 1.6~7.7 $\times$ 10^7 M^{-1}s^{-1} [53], while the rate constant of the reaction between TBA and $\cdot$OH is 3.8~7.6 $\times$ 10^8 M^{-1}s^{-1}, and the rate constant of reaction with SO$_4^-$ is 4~9.1 $\times$ 10^5 M^{-1}s^{-1} [54]. Thus, EtOH is served to quench both SO$_4^{-\cdot}$ and $\cdot$OH, while TBA is specifically employed to quench $\cdot$OH.
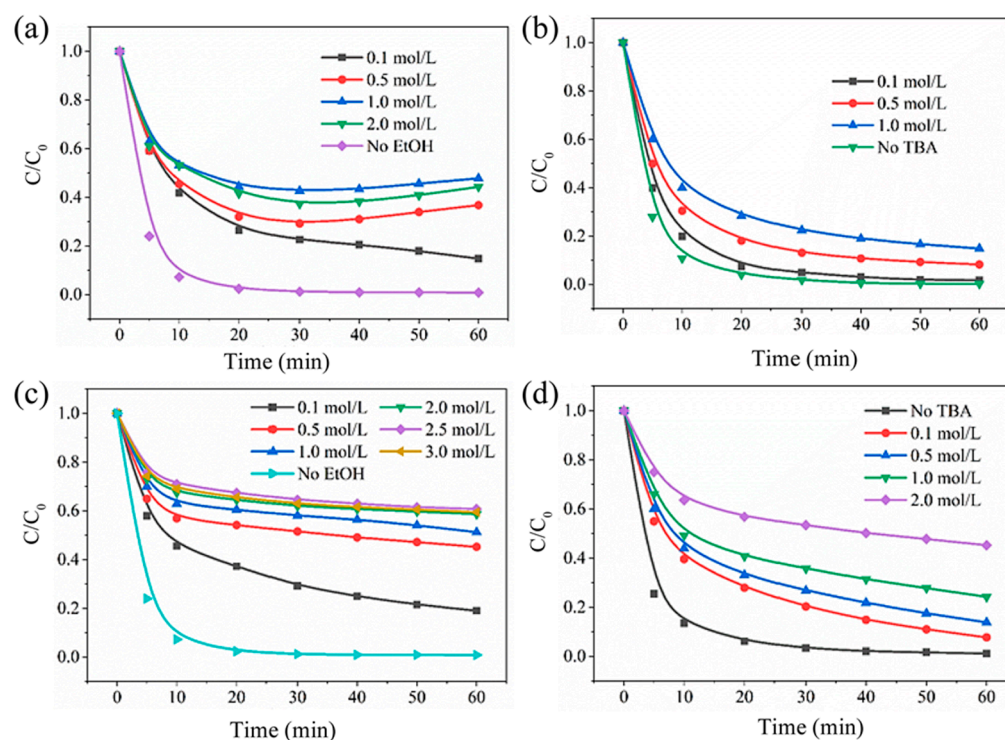
Figure 6. (**a**) Effect of EtOH on acid orange II degradation in the VTM/PDS reaction system. (**b**) Effect of TBA on acid orange II degradation in the VTM/PDS reaction system. (**c**) The influence of EtOH on acid orange II degradation in the VTM/PMS reaction system. (**d**) The influence of TBA on acid orange II degradation in the VTM/PMS reaction system.

In the VTM/PDS system, acid orange II was completely degraded within 60 min without the addition of EtOH or TBA. The introduction of EtOH reduced the degradation efficiency, dropping to 85% with a concentration of 0.1 mM (Figure 6a). TBA exhibited a minimal impact on the degradation of acid orange in the VTM/PDS system, further indicating that SO$_4^{-\cdot}$ was the main active species in the system (Figure 6b). In addition, both EtOH and TBA had similar inhibition effects in the VTM/PMS system, with the degradation rate decreasing to 81% upon the addition of 0.1 mol/L EtOH and to 89% with 0.1 mol/L TBA (Figure 6c). Meanwhile, the degradation rate decreased to 89% when 0.1 mol/L TBA was added (Figure 6d). This suggests that $\cdot$OH plays a critical role in the VTM/PMS reaction system.

To further analyze the degradation of acid orange II in the various reaction systems, the UV–visible spectrum was used during the degradation process (Figure 7). The absorption spectrum of acid orange in aqueous solution mainly consists of four bands: hydrazone at 484 nm, azo at 430 nm, benzene ring at 230 nm, and naphthalene ring at 310 nm [55]. As the reaction progressed, the disappearance of the visible band absorption peak confirmed the destruction of the azo bond. In the VTM/PMS system, a slight increase in absorption peaks at 310 nm and 228 nm was observed, indicating the degradation of the azo structure and the formation of naphthalene and benzene rings.
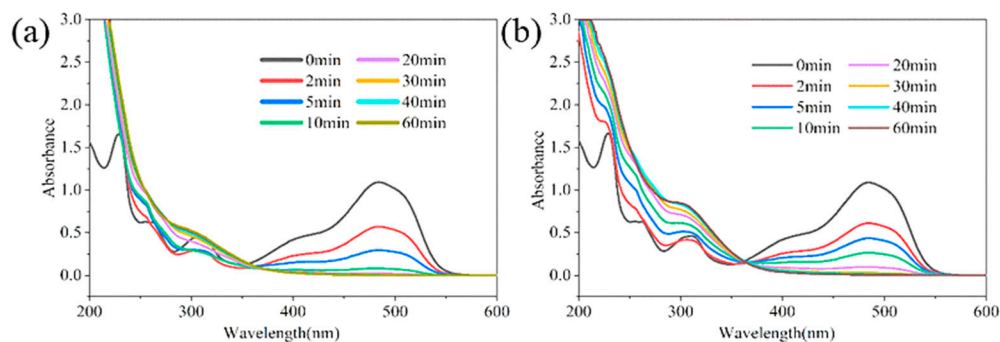
Figure 7. UV-vis analysis of acid orange II in the VTM/PDS reaction system (**a**) and VTM/PMS reaction system (**b**).

4. Conclusions

This study comprehensively investigates differences in the activation performance of VTM on PDS and PMS by determining the degradation of acid orange II. Various persulfates exhibited distinct activation mechanisms for the removal of organic contaminations. Initially, the structure and chemical properties of natural VTM were analyzed, indicating the mesoporous characteristics and multi-metal composition that can facilitate the activation of persulfate catalysts. Subsequently, the degradation of acid orange II was determined, revealing that the degradation efficiency of acid orange II increased with the VTM dosage. When the VTM dosage was 0.2 g/L, the degradation efficiency of acid orange II increased to 75.4%. It is worth noting that excessive VTM inhibited the degradation of acid orange II in persulfate systems, especially in the PDS/VTM system. Extraneous oxidants also affect the degradation performance, such as excess PMS (10 mM), which leads to the self-consumption of free radicals and reduces the reaction efficiency of the system. Temperature and pH were also identified as significant factors affecting persulfate activation. It was found that heating effectively activated PDS but had no impact on PMS at 25 to 55 °C, further proving the greater thermal stability of PMS compared to PDS. The free radical quenching experiments revealed that $SO_4^{-\cdot}$ was the primary active species in the PDS/VTM system, while $\cdot OH$ predominated in the PMS/VTM system. The 0.1 mM EtOH reduced 85% of the degradation efficiency, further indicating that $SO_4^{-\cdot}$ was the main active species in the system. Moreover, the azo bond of acid orange II was the main target of the active substance in the reaction system. The environmental ions, including HCO_3^-, CO_3^{2-}, and HPO_4^{2-}, significantly influenced the degradation of acid orange by changing the pH of the reaction system and consuming the active radicals. This research enhances the understanding of the distinct mechanisms and influencing factors associated with the activation of PDS and PMS by VTM, promoting the optimal application of persulfate in aqueous environments.

Author Contributions: Z.Z.: Investigation, Validation, Formal analysis, Writing—original draft, Writing—review and editing. L.Z.: Writing—review and editing. J.T.: Writing—review and editing. S.R.: Conceptualization, Writing—review and editing. W.Z.: Writing—review and editing, Supervision, Funding acquisition. All authors have read and agreed to the published version of the manuscript.

Data Availability Statement: The original data are available by request from the authors.

Conflicts of Interest: The authors declare that they have no known competing financial interests or personal relationships that could have appeared to influence the work reported in this paper.

References

1. Kanzari, F.; Syakti, A.D.; Asia, L.; Malleret, L.; Piram, A.; Mille, G.; Doumenq, P. Distributions and sources of persistent organic pollutants (aliphatic hydrocarbons, PAHs, PCBs and pesticides) in surface sediments of an industrialized urban river (Huveaune), France. *Sci. Total Environ.* **2014**, *478*, 141–151. [CrossRef]

2. Dsikowitzky, L.; Schwarzbauer, J. Industrial organic contaminants: Identification, toxicity and fate in the environment. *Environ. Chem. Lett.* **2014**, *12*, 371–386. [CrossRef]

3. Garfí, M.; Flores, L.; Ferrer, I. Life Cycle Assessment of wastewater treatment systems for small communities: Activated sludge, constructed wetlands and high rate algal ponds. *J. Clean. Prod.* **2017**, *161*, 211–219. [CrossRef]

4. Miklos, D.B.; Remy, C.; Jekel, M.; Linden, K.G.; Drewes, J.E.; Hübner, U. Evaluation of advanced oxidation processes for water and wastewater treatment—A critical review. *Water Res.* **2018**, *139*, 118–131. [CrossRef]

5. Gahrouei, A.E.; Vakili, S.; Zandifar, A.; Pourebrahimi, S. From wastewater to clean water: Recent advances on the removal of metronidazole, ciprofloxacin, and sulfamethoxazole antibiotics from water through adsorption and advanced oxidation processes (AOPs). *Environ. Res.* **2024**, *252*, 119029. [CrossRef]

6. Shang, Y.; Xu, X.; Gao, B.; Wang, S.; Duan, X. Single-atom catalysis in advanced oxidation processes for environmental remediation. *Chem. Soc. Rev.* **2021**, *50*, 5281–5322. [CrossRef]

7. Aveiro, L.R.; Da Silva, A.G.M.; Candido, E.G.; Antonin, V.S.; Parreira, L.S.; Papai, R.; Gaubeur, I.; Silva, F.L.; Lanza, M.R.V.; Camargo, P.H.C.; et al. Application and stability of cathodes with manganese dioxide nanoflowers supported on Vulcan by Fenton systems for the degradation of RB5 azo dye. *Chemosphere* **2018**, *208*, 131–138. [CrossRef]

8. Nosaka, Y.; Nosaka, A.Y. Generation and Detection of Reactive Oxygen Species in Photocatalysis. *Chem. Rev.* **2017**, *117*, 11302–11336. [CrossRef] [PubMed]

9. Moradi, A.; Kazemeini, M.; Hosseinpour, V.; Pourebrahimi, S. Efficient degradation of naproxen in wastewater using Ag-deposited ZnO nanoparticles anchored on a house-of-cards-like MFI-type zeolite: Preparation and physicochemical evaluations of the photocatalyst. *J. Water Process Eng.* **2024**, *60*, 105155. [CrossRef]

10. Aran-Ais, R.M.; Yu, Y.; Hovden, R.; Solla-Gullon, J.; Herrero, E.; Feliu, J.M.; Abruna, H.D. Identical Location Transmission Electron Microscopy Imaging of Site-Selective Pt Nanocatalysts: Electrochemical Activation and Surface Disordering. *J. Am. Chem. Soc.* **2015**, *137*, 14992–14998. [CrossRef]

11. Oturan, N.; van Hullebusch, E.D.; Zhang, H.; Mazeas, L.; Budzinski, H.; Le Menach, K.; Oturan, M.A. Occurrence and Removal of Organic Micropollutants in Landfill Leachates Treated by Electrochemical Advanced Oxidation Processes. *Environ. Sci. Technol. Lett.* **2015**, *49*, 12187–12196. [CrossRef] [PubMed]

12. Rastogi, A.; Al-Abed, S.R.; Dionysiou, D.D. Sulfate radical-based ferrous–peroxymonosulfate oxidative system for PCBs degradation in aqueous and sediment systems. *Appl. Catal. B Environ.* **2009**, *85*, 171–179. [CrossRef]

13. Giannakis, S.; Lin, K.-Y.A.; Ghanbari, F. A review of the recent advances on the treatment of industrial wastewaters by Sulfate Radical-based Advanced Oxidation Processes (SR-AOPs). *Chem. Eng. J.* **2021**, *406*, 127083. [CrossRef]

14. Ushani, U.; Lu, X.; Wang, J.; Zhang, Z.; Dai, J.; Tan, Y.; Wang, S.; Li, W.; Niu, C.; Cai, T.; et al. Sulfate radicals-based advanced oxidation technology in various environmental remediation: A state-of-the-art review. *Chem. Eng. J.* **2020**, *402*, 126232. [CrossRef]

15. Oh, W.-D.; Dong, Z.; Lim, T.-T. Generation of sulfate radical through heterogeneous catalysis for organic contaminants removal: Current development, challenges and prospects. *Appl. Catal. B Environ.* **2016**, *194*, 169–201. [CrossRef]

16. Devi, P.; Das, U.; Dalai, A.K. In-situ chemical oxidation: Principle and applications of peroxide and persulfate treatments in wastewater systems. *Sci. Total Environ.* **2016**, *571*, 643–657. [CrossRef]

17. Anipsitakis, G.P.; Dionysiou, D.D. Degradation of Organic Contaminants in Water with Sulfate Radicals Generated by the Conjunction of Peroxymonosulfate with Cobalt. *Environ. Sci. Technol.* **2003**, *37*, 4790–4797. [CrossRef] [PubMed]

18. Song, H.; Yan, L.; Wang, Y.; Jiang, J.; Ma, J.; Li, C.; Wang, G.; Gu, J.; Liu, P. Electrochemically activated PMS and PDS: Radical oxidation versus nonradical oxidation. *Chem. Eng. J.* **2020**, *391*, 123560. [CrossRef]

19. Anipsitakis, G.P.; Dionysiou, D.D. Radical Generation by the Interaction of Transition Metals with Common Oxidants. *Environ. Sci. Technol.* **2004**, *38*, 3705–3712. [CrossRef]

20. Ji, Y.; Fan, Y.; Liu, K.; Kong, D.; Lu, J. Thermo activated persulfate oxidation of antibiotic sulfamethoxazole and structurally related compounds. *Water Res.* **2015**, *87*, 1–9. [CrossRef]

21. An, D.; Westerhoff, P.; Zheng, M.; Wu, M.; Yang, Y.; Chiu, C.-A. UV-activated persulfate oxidation and regeneration of NOM-Saturated granular activated carbon. *Water Res.* **2015**, *73*, 304–310. [CrossRef] [PubMed]

22. Anipsitakis, G.P.; Tufano, T.P.; Dionysiou, D.D. Chemical and microbial decontamination of pool water using activated potassium peroxymonosulfate. *Water Res.* **2008**, *42*, 2899–2910. [CrossRef]

23. Wang, J.; Wang, S. Activation of persulfate (PS) and peroxymonosulfate (PMS) and application for the degradation of emerging contaminants. *Chem. Eng. J.* **2018**, *334*, 1502–1517. [CrossRef]

24. Li, Y.; Dong, H.; Li, L.; Tang, L.; Tian, R.; Li, R.; Chen, J.; Xie, Q.; Jin, Z.; Xiao, J.; et al. Recent advances in waste water treatment through transition metal sulfides-based advanced oxidation processes. *Water Res.* **2021**, *192*, 116850. [CrossRef] [PubMed]

25. Shang, W.; Dong, Z.; Li, M.; Song, X.; Zhang, M.; Jiang, C.; Feiyun, S. Degradation of diatrizoate in water by Fe(II)-activated persulfate oxidation. *Chem. Eng. J.* **2019**, *361*, 1333–1344. [CrossRef]

26. Liang, X.; Zhong, Y.; Zhu, S.; Zhu, J.; Yuan, P.; He, H.; Zhang, J. The decolorization of Acid Orange II in non-homogeneous Fenton reaction catalyzed by natural vanadium–titanium magnetite. *J. Hazard. Mater.* **2010**, *181*, 112–120. [CrossRef]

27. Gan, C.-d.; Yang, J.-y.; Du, X.-y.; Li, J.-l.; Tang, Q.-x.; Nikitin, A. Vanadium mobilization and redistribution during mineral transformation of vanadium-titanium magnetite tailings with different weathering degrees. *Sci. Total Environ.* **2023**, *894*, 165068. [CrossRef]

28. Zhang, W.; Tang, G.; Yan, J.; Zhao, L.; Zhou, X.; Wang, H.; Feng, Y.; Guo, Y.; Wu, J.; Chen, W.; et al. The decolorization of methyl orange by persulfate activated with natural vanadium-titanium magnetite. *Appl. Surf. Sci.* **2020**, *509*, 144886. [CrossRef]

29. Chen, X.; Yang, B.; Oleszczuk, P.; Gao, Y.; Yuan, X.; Ling, W.; Waigi, M.G. Vanadium oxide activates persulfate for degradation of polycyclic aromatic hydrocarbons in aqueous system. *Chem. Eng. J.* **2019**, *364*, 79–88. [CrossRef]

30. Fang, G.; Wu, W.; Liu, C.; Dionysiou, D.D.; Deng, Y.; Zhou, D. Activation of persulfate with vanadium species for PCBs degradation: A mechanistic study. *Appl. Catal. B Environ.* **2017**, *202*, 1–11. [CrossRef]

31. Su, Y.; Wu, Z.; Wu, Y.; Yu, J.; Sun, L.; Lin, C. Acid Orange II degradation through a heterogeneous Fenton-like reaction using Fe–TiO2 nanotube arrays as a photocatalyst. *J. Mater. Chem. A* **2015**, *3*, 8537–8544. [CrossRef]

32. Yu, X.; Sun, J.; Li, G.; Huang, Y.; Li, Y.; Xia, D.; Jiang, F. Integration of ●SO4$^-$-based AOP mediated by reusable iron particles and a sulfidogenic process to degrade and detoxify Orange II. *Water Res.* **2020**, *174*, 115622. [CrossRef]

33. Feng, S.; Xiao, B.; Wu, M.; Wang, Y.; Chen, R.; Liu, H. Copper phosphide: A dual-catalysis-center catalyst for the efficient activation of peroxydisulfate and degradation of Orange II. *Sep. Purif. Technol.* **2020**, *248*, 117004. [CrossRef]

34. Lee, J.; von Gunten, U.; Kim, J.-H. Persulfate-Based Advanced Oxidation: Critical Assessment of Opportunities and Roadblocks. *Environ. Sci. Technol.* **2020**, *54*, 3064–3081. [CrossRef]

35. Liang, H.-y.; Zhang, Y.-q.; Huang, S.-b.; Hussain, I. Oxidative degradation of p-chloroaniline by copper oxidate activated persulfate. *Chem. Eng. J.* **2013**, *218*, 384–391. [CrossRef]

36. Johnson, R.L.; Tratnyek, P.G.; Johnson, R.O.B. Persulfate Persistence under Thermal Activation Conditions. *Environ. Sci. Technol.* **2008**, *42*, 9350–9356. [CrossRef]

37. Tian, S.H.; Tu, Y.T.; Chen, D.S.; Chen, X.; Xiong, Y. Degradation of Acid Orange II at neutral pH using Fe2(MoO4)3 as a heterogeneous Fenton-like catalyst. *Chem. Eng. J.* **2011**, *169*, 31–37. [CrossRef]

38. Lv, H.; Ma, L.; Zeng, P.; Ke, D.; Peng, T. Synthesis of floriated ZnFe2O4 with porous nanorod structures and its photocatalytic hydrogen production under visible light. *J. Mater. Chem.* **2010**, *20*, 3665–3672. [CrossRef]

39. Su, M.; He, C.; Sharma, V.K.; Abou Asi, M.; Xia, D.; Li, X.-z.; Deng, H.; Xiong, Y. Mesoporous zinc ferrite: Synthesis, characterization, and photocatalytic activity with H2O2/visible light. *J. Hazard. Mater.* **2012**, *211–212*, 95–103. [CrossRef]

40. Zubir, N.A.; Yacou, C.; Motuzas, J.; Zhang, X.; Diniz da Costa, J.C. Structural and functional investigation of graphene oxide–Fe3O4 nanocomposites for the heterogeneous Fenton-like reaction. *Sci. Rep.* **2014**, *4*, 4594. [CrossRef]

41. Li, Y.; Li, S.; Hu, J.; Zhang, Y.; Du, Y.; Han, X.; Liu, X.; Xu, P. Hollow FeCo-FeCoP@C nanocubes embedded in nitrogen-doped carbon nanocages for efficient overall water splitting. *J. Energy Chem.* **2021**, *53*, 1–8. [CrossRef]

42. Zhang, Y.; Duan, Z.; Jin, Y.; Han, H.; Xu, C. Chemical Bond Bridging across Two Domains: Generation of Fe(II) and In Situ Formation of FeSx on Zerovalent Iron. *Environ. Sci. Technol.* **2023**, *57*, 11336–11344. [CrossRef]

43. Lai, L.; Zhou, H.; Lai, B. Heterogeneous degradation of bisphenol A by peroxymonosulfate activated with vanadium-titanium magnetite: Performance, transformation pathways and mechanism. *Chem. Eng. J.* **2018**, *349*, 633–645. [CrossRef]

44. Pang, Y.; Zhou, X.; Vovk, E.I.; Guan, C.; Li, S.; van Bavel, A.P.; Yang, Y. Understanding lanthanum oxide surface structure by DFT simulation of oxygen 1s calibrated binding energy in XPS after in situ treatment. *Appl. Surf. Sci.* **2021**, *548*, 149214. [CrossRef]

45. Yi, X.; Gao, R.; Liu, X.; Chen, Y.; Zeng, B.; Xu, Y.; Yuan, C.; Dai, L. Phenylenediamine-Guanidine Phosphate Carbon Dots for Flame-Retardant and UV-Resistant Poly(vinyl alcohol) Composite Films. *ACS Appl. Nano Mater.* **2024**, *7*, 13260–13270. [CrossRef]

46. Jiang, M.; Lu, J.; Ji, Y.; Kong, D. Bicarbonate-activated persulfate oxidation of acetaminophen. *Water Res.* **2017**, *116*, 324–331. [CrossRef]

47. Bennedsen, L.R.; Muff, J.; Søgaard, E.G. Influence of chloride and carbonates on the reactivity of activated persulfate. *Chemosphere* **2012**, *86*, 1092–1097. [CrossRef]

48. Cai, C.; Zhang, H.; Zhong, X.; Hou, L. Ultrasound enhanced heterogeneous activation of peroxymonosulfate by a bimetallic Fe–Co/SBA-15 catalyst for the degradation of Orange II in water. *J. Hazard. Mater.* **2015**, *283*, 70–79. [CrossRef]

49. Yang, S.; Wang, P.; Yang, X.; Shan, L.; Zhang, W.; Shao, X.; Niu, R. Degradation efficiencies of azo dye Acid Orange 7 by the interaction of heat, UV and anions with common oxidants: Persulfate, peroxymonosulfate and hydrogen peroxide. *J. Hazard. Mater.* **2010**, *179*, 552–558. [CrossRef]

50. Wacławek, S.; Lutze, H.V.; Grübel, K.; Padil, V.V.T.; Černík, M.; Dionysiou, D.D. Chemistry of persulfates in water and wastewater treatment: A review. *Chem. Eng. J.* **2017**, *330*, 44–62. [CrossRef]

51. Ghauch, A.; Tuqan, A.M.; Kibbi, N. Ibuprofen removal by heated persulfate in aqueous solution: A kinetics study. *Chem. Eng. J.* **2012**, *197*, 483–492. [CrossRef]

52. Ma, J.; Yang, Y.; Jiang, X.; Xie, Z.; Li, X.; Chen, C.; Chen, H. Impacts of inorganic anions and natural organic matter on thermally activated persulfate oxidation of BTEX in water. *Chemosphere* **2018**, *190*, 296–306. [CrossRef]

53. Liu, F.; Yi, P.; Wang, X.; Gao, H.; Zhang, H. Degradation of Acid Orange 7 by an ultrasound/ZnO-GAC/persulfate process. *Sep. Purif. Technol.* **2018**, *194*, 181–187. [CrossRef]

54. Xu, Y.; Ai, J.; Zhang, H. The mechanism of degradation of bisphenol A using the magnetically separable $CuFe_2O_4$/peroxymonosulfate heterogeneous oxidation process. *J. Hazard. Mater.* **2016**, *309*, 87–96. [CrossRef]

55. Yang, S.; Yang, X.; Shao, X.; Niu, R.; Wang, L. Activated carbon catalyzed persulfate oxidation of Azo dye acid orange 7 at ambient temperature. *J. Hazard. Mater.* **2011**, *186*, 659–666. [CrossRef]